A Temperature-Thread Multiscale Modeling Approach for Efficient Prediction of Part Distortion by Selective Laser Melting

C. Li[*], J.F. Liu[*], Y.B. Guo[*], Z.Y. Li[†]
[*]Dept. of Mechanical Engineering, The University of Alabama, Tuscaloosa, AL35487, USA
[†]School of Mechanical Engineering, Shandong University of Technology, Zibo 255049, China

REVIEWED

Abstract

Selective laser melting (SLM) is a powder bed based additive manufacturing process to manufacture functional parts. The high-temperature process will produce large tensile residual stress which leads to part distortion and negatively affect product performance. Due to the complex process mechanism and coupling multi-physics phenomena, the micro-scale single laser scan modeling approach is not practical to predict macro part distortion since it demands an exceedingly long computational time. In this study, a temperature-based multiscale modeling approach has been developed to simulate material phase transition of powder-liquid-solid for fast prediction of part distortion. An equivalent body heat flux obtained from the micro-scale laser scan can be imported as "temperature-thread" to the subsequent layer hatching process. Then the hatched layer with temperature filed can be used as a basic unit to build up the macro-scale part with different scanning strategies. The temperature history and residual stress fields during the SLM process were obtained. In addition, the part distortion can be predicted with a reasonable accuracy by comparing with the experimental data.

***Keywords*:** Selective laser melting, temperature thread, distortion, multiscale simulation

[*] Corresponding author
Tel.: 1-205-348-2615; fax: +1-205-348-6419. E-mail address: yguo@eng.ua.edu

1. Introduction

1.1 SLM process

Selective laser melting (SLM) is a powder bed based additive manufacturing process, which is capable of producing functional parts in a layer upon layer fashion directly from CAD data [1,2]. Unlike other additive manufacturing processes such as selective laser sintering (SLS), SLM is able to produce metal parts with near full density and mechanical properties comparable to those by conventional casting and forming [3,4]. In the past decade, SLM has drawn great attentions in aerospace, automotive, biomedical, and energy industries [5-8].

In a typical SLM experiment setup, a powder layer is placed onto a substrate plate inside a building chamber with an inert atmosphere. A laser is used to fully melt the powder material in the selected area to achieve near full density. After one layer is deposited, another powder layer will be placed and melt until a part is produced. Serval defects usually exist in a SLM part. High temperature gradient due to the rapid heating and cooling generates high thermal stress and leads to part distortion and cracks [9]. Balling effect caused by high viscosity and the surface tension of the molten material may result in very poor surface finish [10]. Also, residual gas content, unmelt powder, and oxidized particle may also lead to porosity of the manufactured component [11,12].

1.2 Part distortion of SLM part

Powder material is locally melted by moving laser during a SLM process. The uneven heat input as well as the rapid cooling of the material would generate large amount of tensile residual stresses in the component. Once the residual stress exceeds the yield point of the material will produce plastic deformation which leads to permanent distortion of the part. Part distortion due to tensile residual stress is one of the major defects of SLM parts. It not only reduces the part geometrical accuracy but also and detrimentally affects the functional performance of the end-use parts. A post processing to fix the distortion would dramatically increases the manufacturing cost. Experimental works have been done to investigate the distribution of the residual stress and the mechanism of part distortion. [13,14]. Several methods have been explored to prevent or reduce part distortion for a SLM process [9,15]. Preheating of the metal powder bed and the substrate is the most widely used method to reduce the part distortion during a SLM process.

1.3 Assessment on current prediction methods

Numerical modeling as a powerful tool has been widely used to predict residual stress and part distortion of the additive manufacturing processes. Simulation works have been done to predict residual stress and distortion of SLM parts on a small domain (usually single track or single wall). Dai *et al.* [16] simulated the effect of powder-to-solid transition to investigate the residual stress and distortion of metal and ceramic powders at the micro-scale. Hodge *et al.* [17] studied the thermal and mechanical history of a SLM process on the meso-scale (12 layers of

powder). A volumetric moving flux was used to melt powder materials with material state change taken into consideration during the process. Aggarangsi *et al.* [18] explored the residual stress reduction method of a SLMed thin-wall structure by using a secondary moving heat flux to preheat the powder material in a finite element model. Heigel *et al.* [19] studied the thermal history and mechanical response of a single wall deposited on a single-side fixed substrate, the deflection history of the substrate was simulated and validated.

Several studies predicted residual stress and part distortion in SLM on the macro-scale. Nickel *et al*. [20] applied a constant heat flux to heat an entire scan line at the same instant. Different scanning patterns were considered to predict the residual stress and distortion. Zaeh *et al.* [21] applied a uniform thermal load adjusted from experimental data to heat up 20 real layers at the same time to predict the temperature and residual stress distribution of a cantilever. Prabhakar *et al.* [22] directly applied a uniform heat source simultaneously to the whole layer to simulate the residual stress formation of tensile test coupons produced by electron beam melting (EBM) as well as the distortion of the substrate.

1.4 Pressing issues and research objective

It should be noted that a coupled thermal-mechanical analysis for several single scans at the micro-scale with a fine mesh model would take many hours or many days to complete, which depends on model size and computer performance. However, a practical SLM part on the macro-scale requires millions of micro-scale laser scans which would dramatically increases the computational load for the numerical calculation of coupled analysis. Thus, it is extremely difficult to predict part distortion of a practical SLM part if every single scan is simulated even using a very powerful work station.

A multi-scale approach is highly needed to achieve acceptable accuracy of part distortion and residual stress with low computational cost. The approach developed in this study divides a SLM process for a practical part into three scales, i.e., micro-scale, meso-scale and macro-scale. At the micro-scale, the material is melt by a single laser scan and the thermal history of the melt pool is recorded. At the meso-scale, the thermal history from the micro scale model is extended to a whole layer. At the macro-scale, a practical part is built layer upon layer by applying the thermal load developed from the meso-scale model. The three different length scales are integrated through the thermal history of the melt material via the "temperature-thread" method. The total number of elements can be reduced dramatically using the multiscale approach. And the total computational time for the integrated three scales is reduced significantly compared to the conventional modeling methods.

The objective of this study is to develop a temperature-thread multi-scale finite element model for efficient prediction of practical SLM part distortion and residual stress by: (a) developing a novel equivalent heat source within a meso-scale model from a micro-scale laser scan model; (b) modeling the power-liquid-solid material state transition during the SLM process; (c) calculating the residual stress field and distortion of a practical part on a macro-scale model; and (d) validating the predicted distortion with the experimental data.

2. SLM Experiment Conditions

2.1 Process parameters

The laser source in this study is a continuous Nd:YAG laser with a wavelength of 1064 nm. The process parameters are listed in Table 1.

Table 1 SLM process parameters

Laser power W	Laser spot diameter μm	Scan speed mm/s	Scan spacing μm	Layer thickness μm
300	600	50	100	150

2.2 Material properties

This study aims to predict part distortion and validate with the experimental data using the lab-made iron-based powders [4]. As the material properties of the powder are not available, a commercial powder from EOS GmbH named DirectSteel® is used to approximate the iron-based powders. The comparison between the iron-based powder and DirectSteel® is listed in Table 2. Temperature-independent mechanical and thermal material properties of DirectSteel® are listed in Table 3. The substrate is a 1 mm thick steel plate.

Table 2 Comparison of chemical composition between iron-based powder and DirectSteel®

Powder material	Fe wt.%	Ni wt.%	Cu wt.%	P wt.%	Ref.
Iron-based powder	62.66	20	15	2.34	[4]
DirectSteel® Powder	59.3 ± 0.4	29.1 ± 1.4	9.6 ± 0.9	1.5 ± 0.1	[23]

Table 3 Material properties of solid DirectSteel® [24]

Elastic Modulus	Poisson's ratio	Tensile strength	Yield strength
GPa	-	MPa	MPa
15.3	0.41	600	400
Melting point	Coefficient of thermal expansion	Thermal conductivity	Specific heat
^{o}C	10^{-6}/K	W/m·K	J/kg·K
1330	9	13	375

3. Multiscale Simulation Methodology

In order to achieve efficient prediction of part distortion and residual stress fields with low computational cost, a temperature-thread based multi-scale finite element method has been developed. The temperature is transferred from the micro-scale model to the macro-scale model using the method. The procedure is shown in Fig. 1.

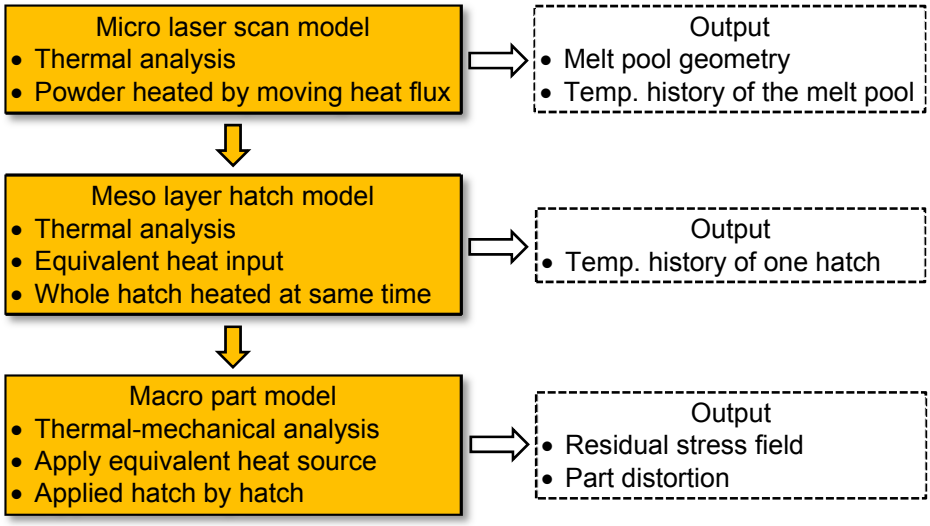

Fig. 1 Temperature-Thread based method for the prediction of distortion of SLM parts.

First, the powder material is melt by a moving heat flux to calculate the temperature field of a molten pool in the micro-scale scan model. Thermal history of the melt pool is recorded. Second, an equivalent heat source is developed based on the thermal history in the micro-scale scan model, then heat load is directly applied to the meso-scale hatch model. Third, the thermal history of one hatch layer is applied to the macro-scale part model, and each hatch layer is activated one by one until the whole part is built.

3.1 Micro Scan Model

Model dimension and mesh

In the micro-scale scan model, the commercial FEA package ABAQUS/Standard was used to perform a thermal analysis to predict the temperature field in the melt pool. Fig. 2 shows the mesh design. A half symmetrical model with respect to the X-Z plane was developed to reduce the computational time. The model consisted of two components: powder layer and substrate. The powder layer was 5 mm in length, 0.3 mm in width and 0.5 mm in thickness and modeled using a fine mesh with an element size of 50 μm (length) × 50 μm (width) × 37.5 μm (thickness). The substrate was 5 mm in length, 0.3 mm in width and 5 mm in height. A relatively coarse mesh for the substrate was used. The initial temperature of powder and substrate was set to room temperature 20 °C.

Heat input modeling

A moving Gaussian distributed heat flux is developed to model the heat input of the scanning laser in the micro-scale model. The Gaussian distributed heat input model was shown in Fig. 2. The heat flux was applied on the top surface of the powder layer by using ABAQUS subroutine DFLUX. The power intensity of heat source is determined by laser absorption coefficient A of the powder material, laser power P, laser spot size d_s and the coordinates of the laser spot center (x, y). The heat flux moves along X direction (see Fig. 2) from point A to point B. The thermal history of the center point of scanning track AB can be recorded.

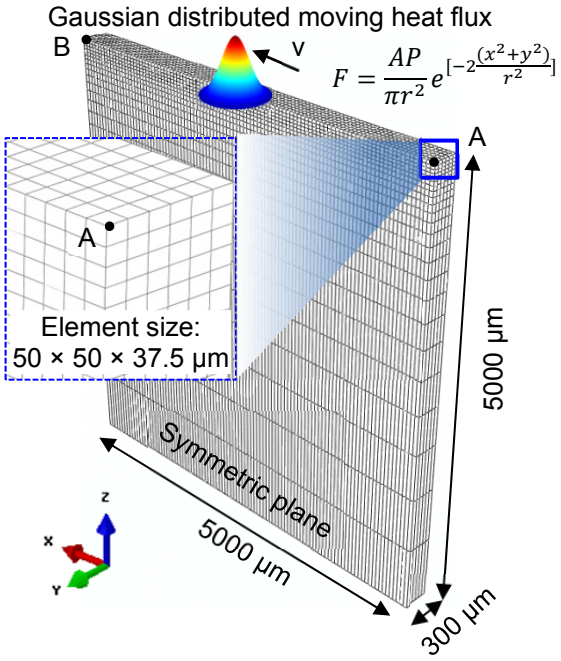

Fig. 2 Model dimension, mesh, and heat input for the micro laser scan model.

Material state transition modeling

The material state transition (powder-liquid-solid) of a SLM process was modeled using ABAQUS subroutine USDFLD. A material state function of the part during the process was defined as f_m, as shown in Fig. 3. The starting material of SLM process in this study is iron-based metal powder, the state function for powder is defined as f_m= 1. After the powder material was melt by laser, the material state was recognized as liquid (f_m= 2). When the material re-solidified after cooling down, the material state function was set to f_m= 3. Different material properties for powder, liquid and solid state were defined based on each corresponding material state functions.

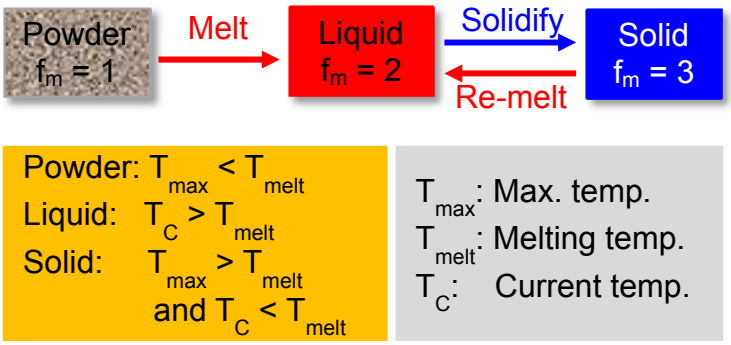

Fig. 3 Modeling of material state transition.

The material state was identified by the current temperature T_c, the maximum temperature T_{max} and the melting temperature T_m of the material. When the maximum temperature of the

material during the entire process is lower than the melting temperature, the material state is identified as powder. When the current temperature of the material is higher than the melting point, the material state is identified as liquid. When the maximum temperature of the material is higher than the melting point while the current temperature is lower than the melting point, the material state is identified as solid.

Temperature history output

Fig. 4(a) shows the temperature contour of the melt pool when the laser is located at the center of the scan track. The thermal history of the melt pool center as shown in Fig. 4(a) is shown in Fig. 4(b). The rapid heating and cooling process of the material which are completed in mini-seconds was achieved.

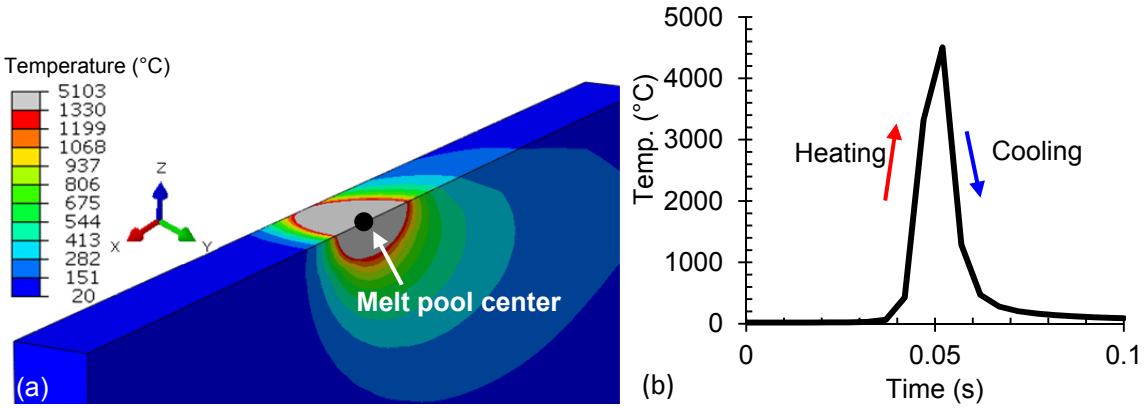

Fig. 4 Temperature contour in the melt pool and temperature history at center of the melt pool.

3.2 Meso Hatch Model

Scan spacing

Scan spacing is an important process parameter in SLM. It determines the length of overlap between two neighboring scan tracks. A large scan spacing would result in unmelt of the metal powders, which could form pores and decrease the density of the part. On the other hand, a small scan spacing represents a higher energy input per unit area, where the metal powder could be molten sufficiently. In this study, the scan spacing was incorporated in the equivalent heat source model. The shape of the melt material underneath the laser spot was semi ellipsoid. In the meso-scale model, it was simplified to a cuboid with a length of laser spot diameter, a width of scan spacing, and a depth of melt pool. The equivalent body flux was defined as the power density (w/m^3) which represents the input power for unit volume of melt material.

Equivalent heat source modeling

Based on the thermal history of the melt pool from the micro-scale model, an equivalent heat source model was developed as shown in Fig. 5. The heat input was modeled by a body heat flux q which is associated with laser power P, laser absorption coefficient A, laser spot diameter d_s, melt pool depth d_m, and hatch spacing H. The body heat flux q was given by Eqn. (1):

$$q = \frac{A \cdot P}{d_s \cdot d_m \cdot H} \tag{1}$$

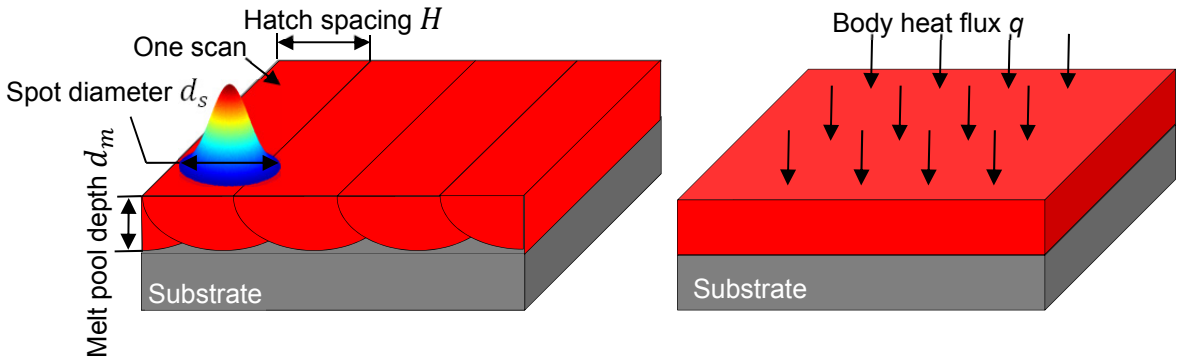

Fig. 5 Equivalent heat source modeling approach for meso layer hatch model.

3.3 Macro Part Model

Model dimension and mesh

In the macro part model, one powder layer was deposited on a substrate. The substrate was a steel plate with the dimensions of 1mm (thickness) × 45 mm (length) 22 mm (width). The part dimensions were 35 mm (length) × 15 mm (width) × 0.15 mm (height) (Fig. 6). In the part region, a fine mesh with an element size of 250 μm (length) × 250 μm (width) × 50 μm (thickness) was used. In the substrate region, a coarse mesh was used to reduce computational time. The initial temperature of powder and substrate was set to 20 °C.

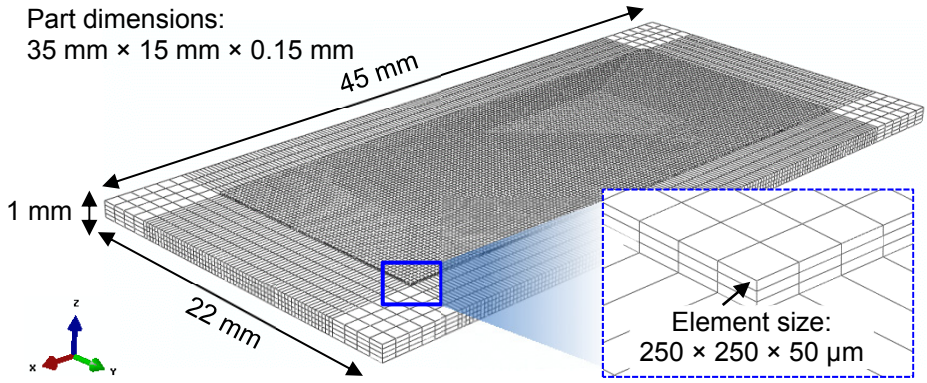

Fig. 6 Mesh design and part dimension in macro part model.

Boundary conditions

Three heat loss mechanisms were considered in the macro part model, i.e., heat conduction to the substrate, the heat convection of the melt pool to the surrounding powder bed and atmosphere, and the heat radiation to the atmosphere. The details of heat transfer modeling were

shown in Fig. 7. In order to simulate the deformation of the part after the SLM process, the two sides were both fixed during the process and then released after the process was finished.

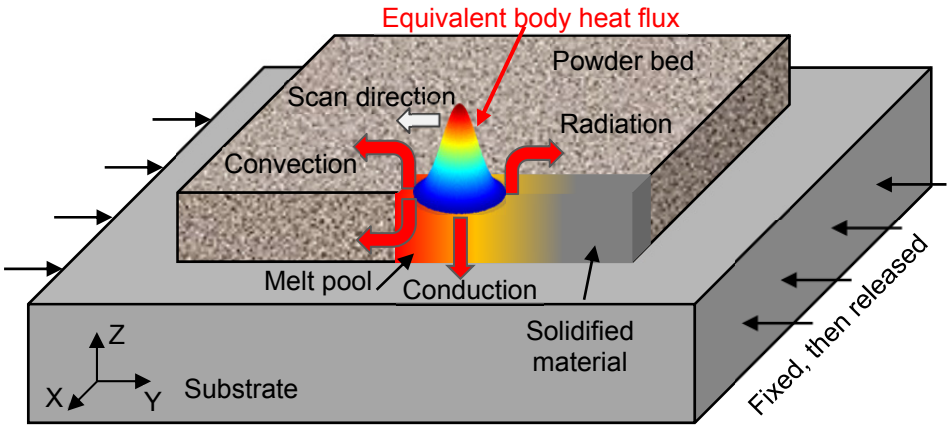

Fig. 7 Heat transfer modeling and boundary conditions in the macro part model.

Part build-up modeling

The scanning strategy in the SLM experiment [4] is a sequential scan pattern (totally 70 scans) as shown in Fig. 8(a). In this study, the sequential pattern was simplified by using an equivalent heat input model as shown in Fig. 8(b). The scanned area was divided into seven zones: from #1 to #7. The #1 zone was heated by the equivalent body heat flux and then cooled down for ten seconds. Same heating strategy was applied to other 6 zones sequentially.

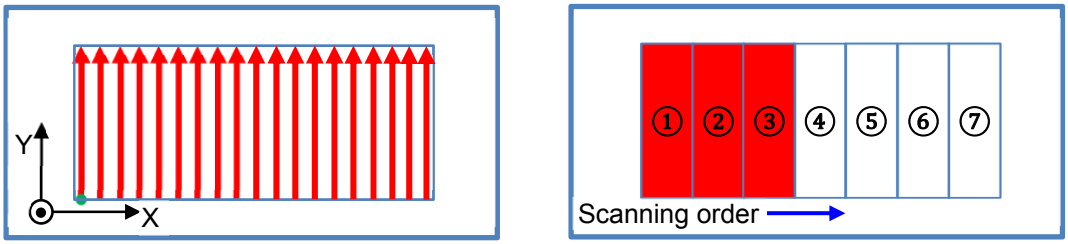

(a) Sequential pattern (vertical scan) (b) Equivalent heat input model

Fig. 8 Scanning pattern applied to the macro part model.

Fig. 9 shows the temperature history of four locations on the top surface of the part. All selected locations were on the boundary of corresponding scanned zones. The first peak temperature for each location was from the heating process of the scanned zone, and the second peak temperature was caused by the heating process of next scanned zone. Since the second peak is higher than material melting temperature, the material located on the boundary of the two neighboring scanned zones will be re-melt during the heating of the next scanned zone.

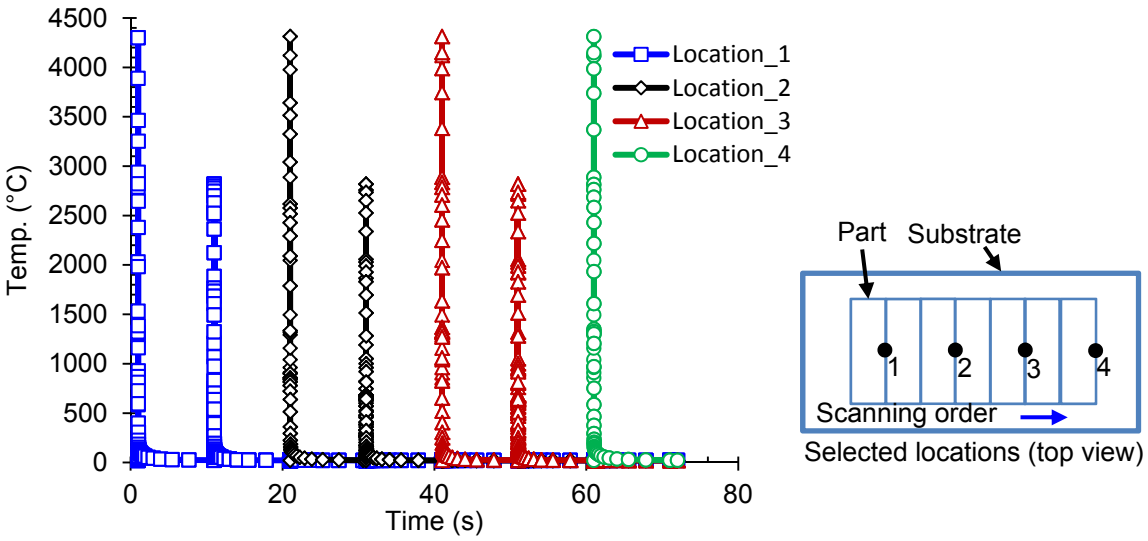

Fig. 9 Temperature history of the selected locations on the top surface of the part.

4. Model Validation and Discussions

4.1 Part distortion

In the experiment, the distortion (in the normal direction of the top surface) of the substrate was measured on the unprocessed side. In the simulation, a nodal path located at the bottom surface of the substrate along the distortion direction (Z) was created as shown in the dash line in Fig. 10. The distortion in the Z direction along this nodal path was normalized and compared to the measurement (Fig. 10). The prediction and experimental data show a similar bending trend. A concave up shape curve was observed. The formation of this curve is due to the thermal history of the part and the substrate. At first, the material located in the upper layer of the part expanded because of the laser heating. As the material cools down, the plastic strain in the upper layers became smaller than the lower layers. Finally, a concave shaped distortion was formed.

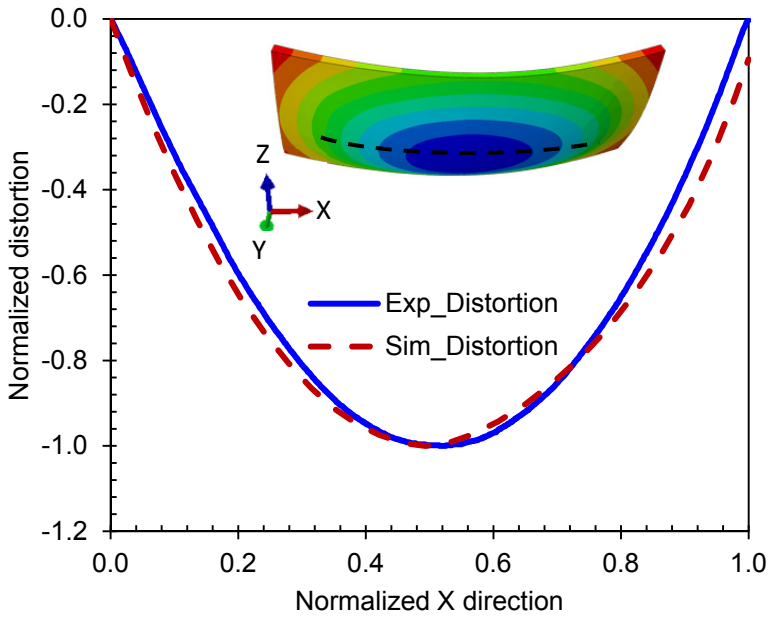

Fig. 10 Part distortion prediction vs. the experimental data.

Fig. 11 shows the distortion history for the center location of the substrate bottom surface during the entire SLM process. A maximum distortion value of 0.35 mm was observed. Seven peaks in the plot represent seven heating processes for each hatch. The followed seven flat lines as shown in Fig. 11 mean the cooling process of the model. During every heating process, the bottom surface moves towards the laser beam (+ Z direction). During the every cooling process, the bottom surface moves away from the laser beam (- Z direction).

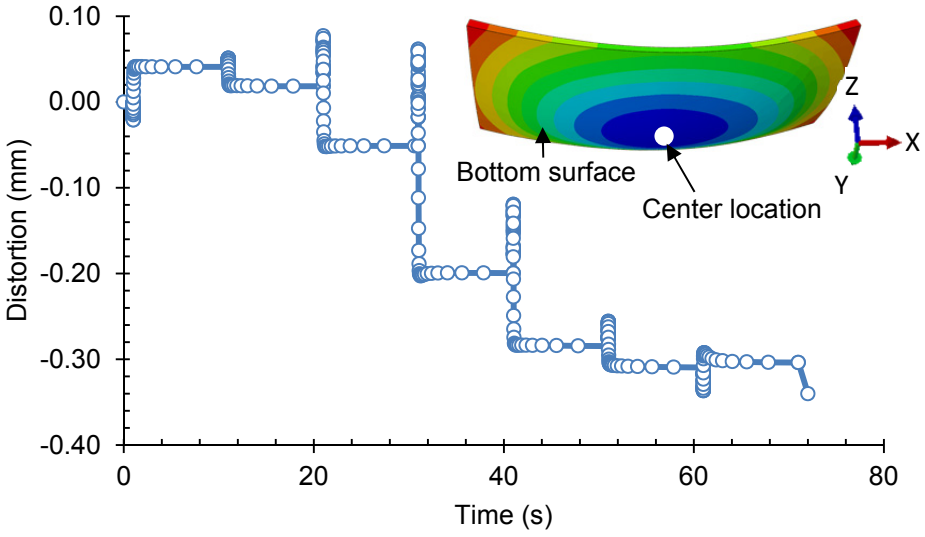

Fig. 11 Distortion history for the center location of the bottom surface.

4.2 Residual stress

Fig. 12 shows the von Mises residual stress contour and Fig. 13 shows the six stress tensor components of the part residual stress after cooling down to room temperature. The maximum von Mises stress (583 MPa) is located on the top surface of the part. And it is higher than the yield point which means plastic deformation occurs after the process. Stress concentration was observed at the edge of the part.

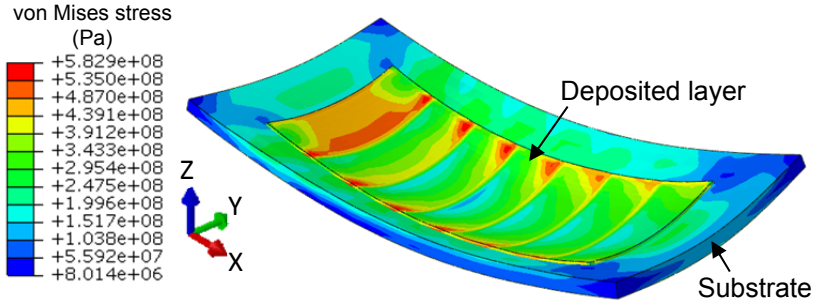

Fig. 12 von Mises stress contour of the part after cooling down to room temperature.

Large amount of tensile residual stresses in X and Y direction were observed on the top surface of the part as shown in Fig. 13(a) and Fig. 13(b). The residual shear stresses S_{33}, S_{12}, S_{13}, and S_{23} were negligible compared to the normal residual stresses S_{11} and S_{22}. It is because most of the deformation of the part and substrate occurred in X and Y direction.

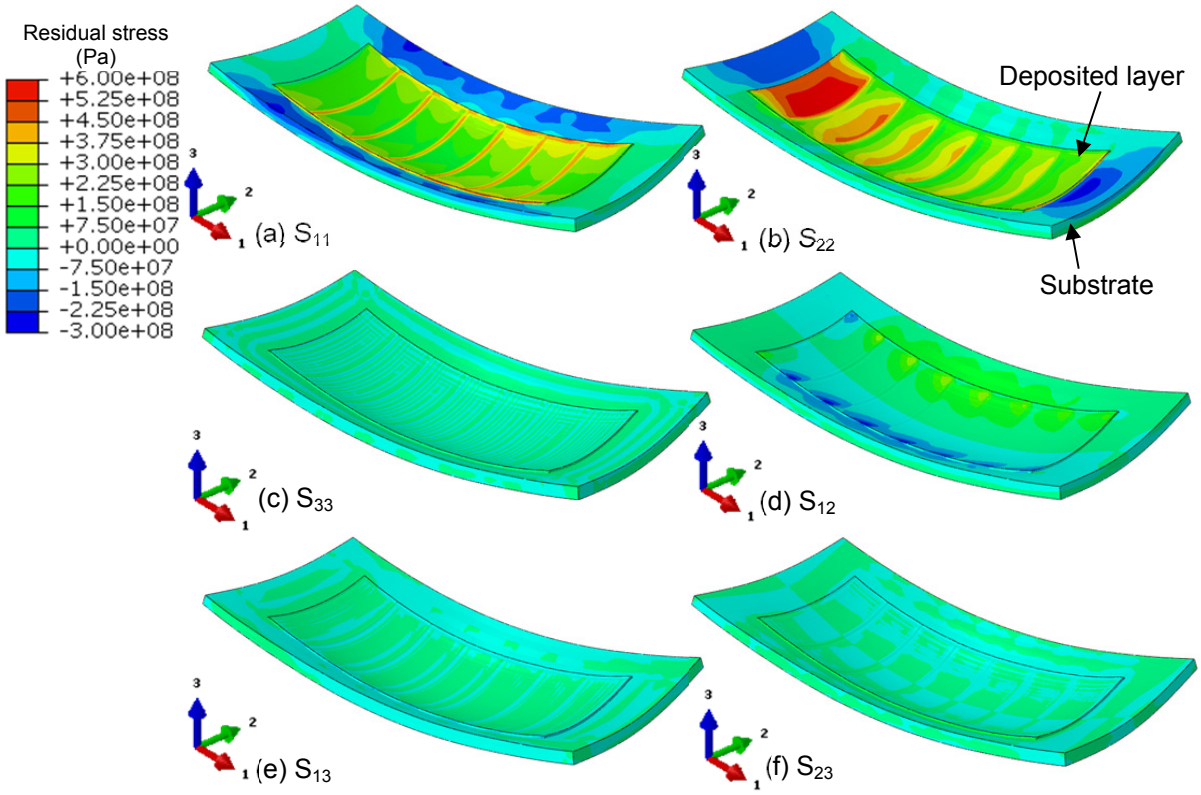

Fig. 13 Residual stress contours (w. substrate).

Fig. 14(a) shows residual stress S_{11} profile in depth direction. The node path was located at the center of the model. The maximum tensile residual stress was found on the top surface of the part, and the tensile stress decreases as the depth increases. A sudden change of residual stress (S_{11}) was found on the boundary between the part and substrate, changing from tensile (+240 MPa) on the part to compressive (-170 MPa) on the substrate. The predicted residual stress profile was very similar to the typical simplified residual stress profile in depth direction [13].

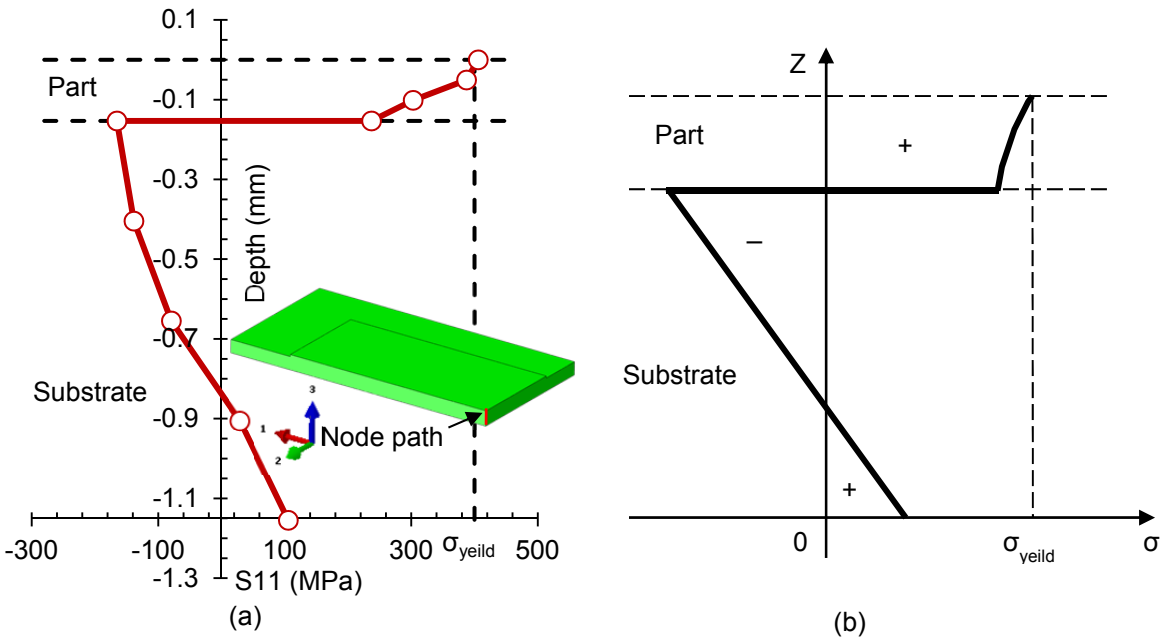

Fig. 14 Residual stress profile in depth direction: (a) predicted residual stress profile and the node path; (b) simplified residual stress profile on a substrate (redraw from [13]).

5. Conclusions

A temperature-thread based multiscale modeling approach has been developed for efficient prediction of part distortion in SLM. Thermal information has been transferred through the micro-scale laser scanning to meso-scale layer hatching and the macro-scale part build-up. The predicted distortion was verified by the experimental data. The key findings are summarized as follows:

- An equivalent heat source has been developed from the thermal history of melt pool in micro-scale laser scanning model and applied to the meso-scale hatch layer, which are incorporated in the macro-scale part to predict part distortion.
- The material state transition phenomenon (powder-liquid-solid) during the SLM process was modeled using different field functions based on the material's current temperature, maximum temperature, and melting temperature.
- Tensile residual stress with a value near the yield point of the material was found on the top surface of the part. A typical residual stress profile in depth direction for a SLMed part was predicted.

6. Acknowledgment

Dr. Z.Y. Li would like to thank the Taishan Scholar Program for support of the collaborative research.

7. References

[1] Kruth J, Leu M, Nakagawa T (1998) Progress in Additive Manufacturing and Rapid Prototyping. *CIRP Annals-Manufacturing Technology* 47(2):525-540.

[2] Levy GN, Schindel R, Kruth J (2003) Rapid Manufacturing and Rapid Tooling with Layer Manufacturing (LM) Technologies, State of the Art and Future Perspectives. *CIRP Annals-Manufacturing Technology* 52(2):589-609.

[3] Kruth J, Levy G, Klocke F, Childs T (2007) Consolidation Phenomena in Laser and Powder-Bed Based Layered Manufacturing. *CIRP Annals-Manufacturing Technology* 56(2):730-759.

[4] Kruth J, Froyen L, Van Vaerenbergh J, Mercelis P, Rombouts M, Lauwers B (2004) Selective Laser Melting of Iron-Based Powder. *J. Mater. Process. Technol.* 149(1):616-622.

[5] Vandenbroucke B, Kruth J (2007) Selective Laser Melting of Biocompatible Metals for Rapid Manufacturing of Medical Parts. *Rapid Prototyping Journal* 13(4):196-203.

[6] Clare AT, Chalker PR, Davies S, Sutcliffe CJ, Tsopanos S (2008) Selective Laser Melting of High Aspect Ratio 3D Nickel–titanium Structures Two Way Trained for MEMS Applications. *International Journal of Mechanics and Materials in Design* 4(2):181-187.

[7] Hollander DA, Von Walter M, Wirtz T, Sellei R, Schmidt-Rohlfing B, Paar O, Erli H (2006) Structural, Mechanical and in Vitro Characterization of Individually Structured Ti–6Al–4V Produced by Direct Laser Forming. *Biomaterials* 27(7):955-963.

[8] Rochus P, Plesseria J, Van Elsen M, Kruth J, Carrus R, Dormal T (2007) New Applications of Rapid Prototyping and Rapid Manufacturing (RP/RM) Technologies for Space Instrumentation. *Acta Astronaut.* 61(1):352-359.

[9] Shiomi M, Osakada K, Nakamura K, Yamashita T, Abe F (2004) Residual Stress within Metallic Model made by Selective Laser Melting Process. *CIRP Ann. Manuf. Technol.* 53(1):195-198.

[10] Tolochko NK, Mozzharov SE, Yadroitsev IA, Laoui T, Froyen L, Titov VI, Ignatiev MB (2004) Balling Processes during Selective Laser Treatment of Powders. *Rapid Prototyping Journal* 10(2):78-87.

[11] Lewis GK, Schlienger E (2000) Practical Considerations and Capabilities for Laser Assisted Direct Metal Deposition. *Mater Des* 21(4):417-423.

[12] Dadbakhsh S, Hao L, Sewell N (2012) Effect of Selective Laser Melting Layout on the Quality of Stainless Steel Parts. *Rapid Prototyping Journal* 18(3):241-249.

[13] Kruth J, Deckers J, Yasa E, Wauthlé R (2012) Assessing and Comparing Influencing Factors of Residual Stresses in Selective Laser Melting using a Novel Analysis Method. *Proc. Inst. Mech. Eng. Pt. B: J. Eng. Manuf.* 226(6):980-991.

[14] Mercelis P, Kruth JP (2006) Residual Stresses in Selective Laser Sintering and Selective Laser Melting. *RAPID PROTOTYPING JOURNAL* 12(5):254-265.

[15] Buchbinder D, Meiners W, Pirch N, Wissenbach K, Schrage J (2014) Investigation on Reducing Distortion by Preheating during Manufacture of Aluminum Components using Selective Laser Melting. *J. Laser Appl.* 26(1):1-10.

[16] Dai K, Shaw L (2004) Thermal and Mechanical Finite Element Modeling of Laser Forming from Metal and Ceramic Powders. *Acta Materialia* 52(1):69-80.

[17] Hodge N, Ferencz R, Solberg J (2013) Implementation of a Thermomechanical Model in Diablo for the Simulation of Selective Laser Melting. Report, Lawrence Livermore National Laboratory, Livermore, CA.

[18] Aggarangsi P, Beuth JL (2006) Localized Preheating Approaches for Reducing Residual Stress in Additive manufacturing. *In Proc. SFF Symp* 709-720.

[19] Heigel JC, Michaleris P, Reutzel EW (2015) Thermo-Mechanical Model Development and Validation of Directed Energy Deposition Additive Manufacturing of Ti–6Al–4V. *Additive Manufacturing* 5(0):9-19.

[20] Nickel A, Barnett D, Prinz F (2001) Thermal Stresses and Deposition Patterns in Layered Manufacturing. *Materials Science and Engineering: A* 317(1):59-64.

[21] Zaeh MF, Branner G (2010) Investigations on Residual Stresses and Deformations in Selective Laser Melting. *Production Engineering* 4(1):35-45.

[22] Prabhakar P, Sames WJ, Dehoff R, Babu SS (2015) Computational Modeling of Residual Stress Formation during the Electron Beam Melting Process for Inconel 718. *Additive Manufacturing*.

[23] Rombouts M (2006) Selective Laser Sintering/Melting of Iron-Based Powders. *Katholieke Universiteit Leuven* .

[24] EOS GmbH (2004) Direct Metal and DirectSteel Materials for EOSINT M 250 Xtended.